J. Fluid Mech. (2007), *vol.* 570, *pp.* 479–489.
doi:10.1017/S0022112006003181 Printed in the United Kingdom

Multi-point local temperature measurements inside the conducting plates in turbulent thermal convection

By CHAO SUN AND KE-QING XIA

Department of Physics, The Chinese University of Hong Kong, Shatin, Hong Kong, China

(Received 17 July 2006 and in revised form 12 September 2006)

An experimental study of local temperature statistics in turbulent thermal convection is presented. The emissions of plumes and plume clusters are detected by an array of thermistors embedded in the top and bottom plates of a 1 m diameter convection cell. We found that the product $S_T S_{T'}$ of the temperature skewness S_T and the skewness of the temperature time derivative $S_{T'}$ from the embedded thermistors may be used as a measure of the intensity of plume emissions and that $S_T S_{T'}$ exhibits a pattern that corresponds well to the orientation of the large-scale circulation in the convecting flow. This is despite the fact that the temperature distribution across the plates is highly uniform, as indicated by the mean temperature of the embedded thermistors. By comparing the spatial distributions of $S_T S_{T'}$ and of the RMS temperature σ, we further find that the maximum temperature fluctuations take place in regions dominated by plume mixing instead of regions of plume emission. It is also found that temperature fluctuations inside the conducting plates have the same statistical and scaling properties as those in the cell centre.

1. Introduction

Turbulent Rayleigh–Bénard convection has attracted much interest during the past decade, partly due to its relevance to astrophysical and geophysical phenomena such as solar and mantle convection and partly because it is an ideal system in which to study thermal turbulence in a closed box. In turbulent convection, the flow is initiated and maintained by the buoyancy force produced by an applied constant temperature difference across the height of a convection cell. The dynamics of the flow is characterized by the geometry of the cell and two control parameters, namely the Rayleigh number, defined as $Ra = \alpha g \Delta H^3/\nu\kappa$ and the Prandtl number, defined as $Pr = \nu/\kappa$. Here g is the gravitational acceleration, Δ the temperature difference between the bottom and the top plates of a convection cell of height H, and α, ν and κ, respectively, the thermal expansion coefficient, kinematic viscosity and thermal diffusivity of the convecting fluid. Another parameter is the aspect ratio Γ, defined as the lateral dimension of the fluid layer over its height. Ra may be understood as the ratio of the buoyancy force driving the flow and the dissipative forces damping it, and Pr is a measure of the relative strengths of momentum and thermal diffusions.

At sufficiently high values of Ra, a large-scale circulation (LSC) is formed across the height of the convection cell (Krishnamurti & Howard 1981). This large-scale circulation, also known as the 'wind' in turbulent convection, has been studied extensively in recent years. Many experimental, theoretical and numerical investigations have been carried out to study the various aspects of the LSC (see, for example,

Xi, Zhou & Xia 2006, which contains a large compilation of relevant references). A prominent coherent object in turbulent convection is the thermal plume that is emitted intermittently from the boundary layers of the conducting plates. Because of the important role played by the plumes in turbulent thermal convection there have been quite a number of recent studies on their properties (Zhou & Xia 2002; Funfschilling & Ahlers 2004; Bershadskii *et al.* 2004; Ching *et al.* 2004; Parodi *et al.* 2004). However most of these studies extracted plume information from measured temperature and velocity fields either in the bulk fluid or near, but outside, the boundary layer. We now know that once the plumes leave the boundary layer their motion is organized spatially via LSC, which in turn is driven and sustained by the plumes themselves in an interactive fashion (Xi, Lam & Xia 2004). An interesting question therefore is how the thermal plumes are distributed spatially initially. In other words, are the plumes emitted uniformly across the conducting plates of the convection cell and then organized spatially by the LSC, or has their emission a certain spatial distribution that corresponds to the flow pattern of the LSC? To answer this question one may need to conduct multi-point measurements either inside or very close to the thermal boundary layer. However, placing too many probes in the convecting fluid inevitably disturbs the turbulent flow. One way to solve this problem is to place a temperature probe inside the conducting plate sufficiently close to the fluid-contact surface so that it senses temperature fluctuations related to plume emissions. Using multiple such probes embedded in the bottom plate of a mercury convection cell Cioni, Ciliberto & Sommeria (1997) have studied the azimuthal motion of the LSC. In order to map out the two-dimensional plume emission pattern requires the use of more probes, which may affect the temperature uniformity in the plate itself. The large area of the 1 m diameter convection cell constructed recently in our laboratory (Sun *et al.* 2005*a*) affords us the opportunity to probe the spatial distribution of plume emissions. Because of the large ratio of the plate area to the thermistor size, one can embed a large number of temperature probes in the plate so that the overall temperature distribution can be obtained while keeping the perturbation to a minimum.

The ability of an embedded temperature probe to sense thermal plume emissions is a manifestation of the effect of the finiteness of the thermal conductivity of the plates, which has received considerable attention recently. Chaumat, Castaing & Chillà (2002) and Hunt *et al.* (2003) considered this analytically, Verzicco (2004) derived an empirical correction formula for it, and Brown *et al.* (2005*b*) experimentally measured this effect. The physical reason for this phenomenon is that the plates can no longer maintain a constant temperature when plumes are emitted. When a hot plume is emitted from the bottom plate, it leaves a 'cold spot' there for a finite time before the temperature recovers to the previous value by conduction. An analogous process occurs at the top plate: the emission of a cold plume will leave a 'hot spot' there for a finite time. The presence of this effect diminishes heat transport compared to a hypothetical plate with infinite thermal conductivity. However, in the present work we take advantage of it by using embedded thermistors to detect the emission and organization of thermal plumes.

2. Experimental apparatus and methods

The convection apparatus has been described in detail in Sun *et al.* 2005. Here we give only its main features. The top and bottom plates of the cell are made of pure copper 3 cm in thickness and their fluid-contact surfaces are plated with a thin layer

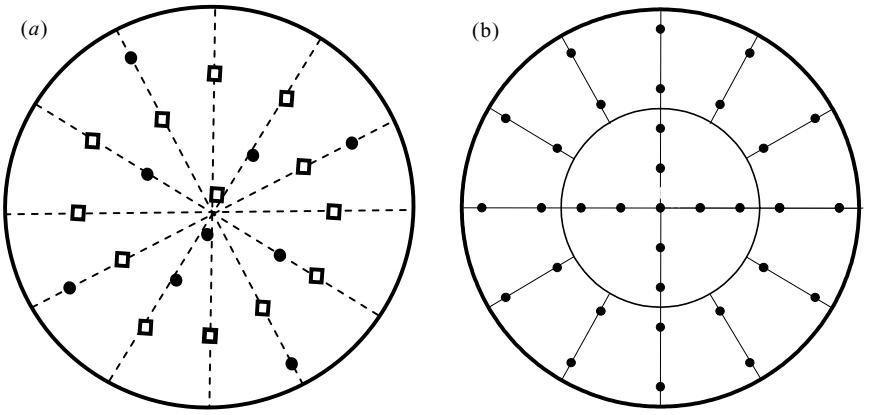

FIGURE 1. Thermistor distributions in (*a*) the top plate and (*b*) the bottom plate. The thermistors denoted by the black dots are 5 mm from the fluid-contact surface of the plates, and those marked by squares are 2 mm from the plate surface. Note that due to the presence of the spiral water cooling channels, the thermistors in the top plate are not positioned on concentric circles.

of nickel. A Plexiglas tube of 100 cm in inner diameter and 2.5 cm in wall thickness is used as the sidewall. Six cylindrical tubes of heights 5.00, 10.10, 20.02, 49.0, 99.9 and 149.4 cm are used in the experiment. The corresponding aspect ratios are $\Gamma =$ 20.00, 9.90, 5.00, 2.04, 1.00 and 0.67, respectively. The change of cell height enabled us to vary the Rayleigh number in the experiment over a wide range. Distilled and degassed water was used as convecting fluid. During the experiment Pr was maintained at 4.3.

Two types of thermistors are used in the present study. Those embedded in the plates have a diameter of 2.4 mm (Model 44031, OMEGA Engineering, Inc.). They have accuracy of 0.02 °C and a time constant of 1 s. The ones (Model AB6E3-B07, GE, Inc.) used for local temperature measurements inside the fluid have a diameter of about 300 μm, an in-water time constant of 10 ms, and an accuracy of 0.01 °C. All thermistors were calibrated individually over the range of temperature measurement. The resistances were measured using a $6\frac{1}{2}$-digit multimeter with 56 channels (HP Model 34970A). The spatial distributions of the thermistors inside the top and bottom plates are shown in figures 1(*a*) and 1(*b*) respectively. In figure 1(*b*) the 16 aluminum heaters (12 in the shape of a sector and 4 as quadrants) are also indicated (see Sun *et al.* 2005*a* for details). Thirty-three thermistors are embedded in the bottom plate and twenty-one in the top plate. Most are placed 5 mm from the fluid-contact surface, while 15 in the top plate are 2 mm from the fluid-contact surface, marked as white squares in figure 1(*a*). These were used only in the measurements with the $\Gamma = 1$ cell. For local temperature measurements in the convecting fluid, three thermistors attached to stainless steel tubes are inserted into the cell from filling stems (see Lui & Xia 1998 for details), one at the cell centre and two on the sidewalls, opposite each other, all at mid-height. Each time Ra is changed it takes about 3 to 10 h for the system to reach the steady state and we typically wait for over 10 h to start the measurements. A typical measurement is averaged over 10 h and more than 20 h for low Δ (< 4°C). It has been previously shown that the temperature distributions in the plates are quite uniform: the time-averaged temperature of any one thermistor deviates less than 1 % from the spatially averaged mean temperature of the plate (Sun *et al.* 2005*a*).

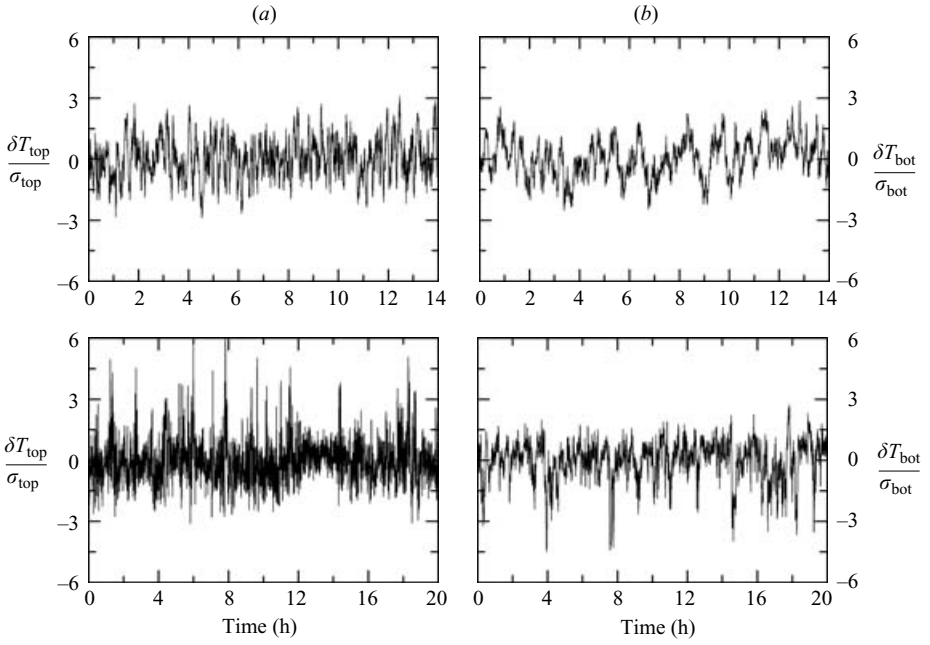

FIGURE 2. Normalized temperature fluctuations measured inside the top (a) and bottom (b) plates. Upper panels are for $Ra = 5.7 \times 10^7$ (in $\Gamma = 20$ cell) and lower panels $Ra = 1.6 \times 10^{11}$ (in $\Gamma = 1$ cell).

3. Results and discussion

3.1. *Signatures of plume emissions inside conducting plates*

Figure 2 plots the time series of the normalized temperature fluctuations $\delta T/\sigma$ measured in the top and the bottom plates for two different Rayleigh numbers, where $\delta T = T(t) - \langle T \rangle$ and σ is the standard deviation of $T(t)$. Here $\langle \cdots \rangle$ denotes time average. The results for both plates are measured by thermistors located about midway between cell centre and the perimeter. The figure shows that at lower Ra the temperature fluctuates rather symmetrically around the mean and the fluctuations are confined mostly to two standard deviations (2σ). On the other hand, at high Ra the fluctuations are rather asymmetric with large spikes that can reach 4σ, and the temperature in the bottom plate is skewed towards low temperature and that in top is skewed to high temperature. These are the signatures of emissions of plumes or clusters of plumes , i.e. the departure of a plume from the plate creates a temperature deficit there. As already mentioned, this finite conductivity effect ultimately reduces heat transfer, which has been discussed by others at the level of global heat transport. Here we provide more direct evidence of it at the local level. It should be noted that the temperature time series for different Ra are measured in cells of different Γ and we assume here that the different behaviour reflects more the difference in Ra than the difference in Γ, as the probes, being imbedded in the plates, are more sensitive to local properties.

The different properties of temperature fluctuations at low and high Ra can also be analysed from their probability density functions (PDF). Figure 3 plots the PDFs of the same temperature time series as in figure 2. For comparison, temperature PDFs measured at the cell centre are also shown. The most striking feature revealed by the figure is that at high values of Ra temperature fluctuations in the cell interior and

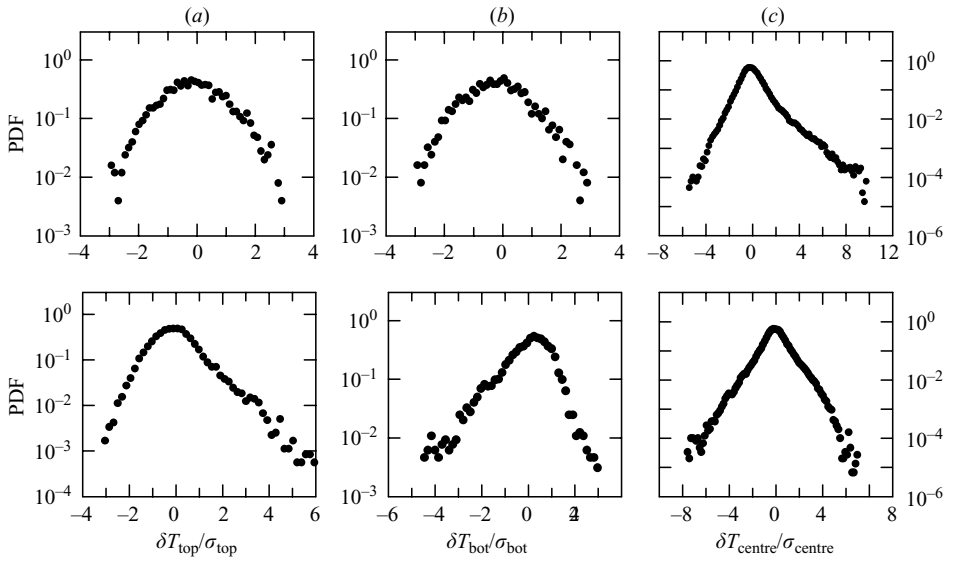

FIGURE 3. PDFs of normalized temperature fluctuations measured inside the top (*a*) and bottom (*b*) plates and (*c*) at the cell centre. Upper panels are for $Ra = 5.7 \times 10^7$ and lower panels $Ra = 1.6 \times 10^{11}$.

inside the plates are qualitatively the same, whereas at low *Ra* they are qualitatively different. It is seen that the PDFs measured inside the plates are Gaussian-like at lower *Ra* and have exponential-like tails at high *Ra*. In contrast, those at the cell centre are exponential-like for both low and high values of *Ra*. At high *Ra* the skewness of the PDFs from the plates is also consistent with the behaviour of temperature fluctuations seen in figure 2. Note that the cell-centre PDF at high *Ra* is more symmetric than that at low *Ra*. Work in progress suggests that this is probably because the former is from a $\Gamma = 1$ cell and has single-roll LSC while the latter is from a $\Gamma = 20$ cell which has a multiroll flow structure.

As temperature fluctuations in the conducting plates clearly show signatures of plumes at high *Ra*, they should share some common features with those in the convecting fluid. In figure 4 we examine the *Ra*-dependence of the normalized temperature root-mean-square (RMS) at the high end of the *Ra* range ($\Gamma = 1$ cell) for data measured at cell centre and inside the plates, where spatial averages of all embedded thermistors in the respective plates are used. The top plate result shows less scatter than the bottom one, which is presumably because some top plate thermistors are closer to the fluid than those in the bottom and therefore have better signal-to-noise ratios. The solid lines in the figure are power-law fits to the respective data: $\sigma/\Delta \sim Ra^{-0.14\pm0.02}$ (centre), $\sigma/\Delta \sim Ra^{-0.11\pm0.04}$ (bottom), and $\sigma/\Delta \sim Ra^{-0.12\pm0.03}$ (top). We note that the cell centre exponent (-0.14) is consistent with a number of previous experimental results (Castaing *et al.* 1989; Xia & Lui 1997); it is also very close to the $-1/7$ derived in the scaling model for turbulent convection by Castaing *et al.* (1989). Because of the limited range in *Ra* the fitted exponents should be taken as only indications of the underlying qualitative behaviour. Nevertheless these results are significant. They show that within the experimental uncertainties temperature fluctuations inside the plates and at the cell centre have approximately the same *Ra*-dependence, and those inside the plates have larger magnitude. The fact that the scaling exponent for the plates

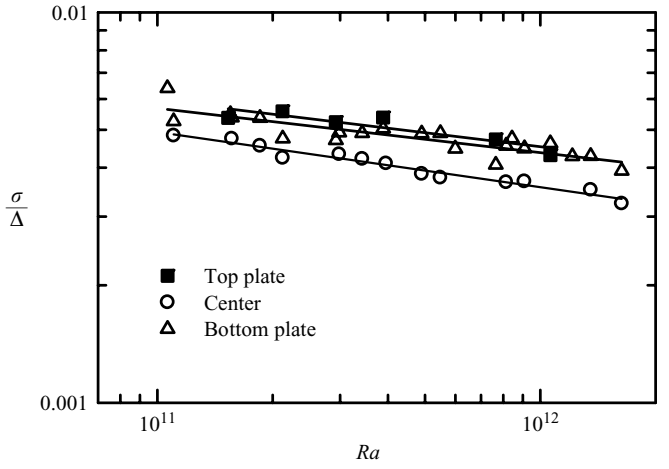

FIGURE 4. Normalized RMS temperature fluctuations σ/Δ measured by the centre and embedded thermistors. The solid lines are power-law fits (see text).

is very close to the centre result implies that there is a single local temperature scale in the system. Because the embedded probes are presumably more sensitive to emissions of plumes or plume clusters and less sensitive to 'background' turbulent fluctuations in the convecting bulk fluid due to shielding of the thermal boundary layer, we may argue that the scaling behaviour of σ/Δ at the cell centre is also dominated by contributions from plumes.

3.2. *Intensity and spatial distribution of plume emissions*

Thermal plumes are believed to originate from the intermittent pinch off of thermal boundary layers which gives rise to the sharp fronts or gradients of the temperature field. Thus a more sensitive quantity to extract the signatures of plumes from the measured temperature time series is its time derivative, as it amplifies the high-frequency components of the temperature signal that correspond to the sharp fronts or gradients. From figures 2 and 3 we also see that temperature fluctuations are highly asymmetric at large *Ra*, because individual plumes are either hot or cold objects compared to their surroundings. This asymmetry may be quantified by the skewness of the temperature field. Belmonte & Libchaber (1996) have identified thermal fronts, or plumes from temperature signals using the skewness of the temperature and of the temperature time derivative. Using skewness of the plus and minus temperature increments, Zhou & Xia (2002) were able to quantify the mixing zone and its evolution with *Ra* in convective flow. They also successfully extracted single thermal plumes from temperature time series at various positions in the cell and found that their size has an approximate log-normal distribution.

The skewnesses of temperature and of its time derivative are defined as

$$S_T = \frac{\langle (T - \langle T \rangle)^3 \rangle}{[\langle (T - \langle T \rangle)^2 \rangle]^{3/2}}, \tag{3.1}$$

$$S_{T'} = \frac{\langle (\partial T/\partial t)^3 \rangle}{[\langle (\partial T/\partial t)^2 \rangle]^{3/2}}. \tag{3.2}$$

In the calculation of $S_{T'}$ we have approximated the temperature time derivative $\partial T/\partial t$ as $dT_i = (T_{i+1} - T_{i-1})/2$ using the discrete time series $\{T_i\}$ (Belmonte &

Ra	5.7×10^7		1.1×10^{11}	
	top	bottom	top	bottom
S_T	0.12	−0.16	0.90	−0.96
$S_{T'}$	0.15	−0.19	0.60	−0.54
$S_T S_{T'}$	0.02	0.03	0.54	0.52

TABLE 1. Values of temperature skewness S_T, the skewness $S_{T'}$ of the temperature time derivative, and their product $S_T S_{T'}$ calculated from the same data as shown in figure 2.

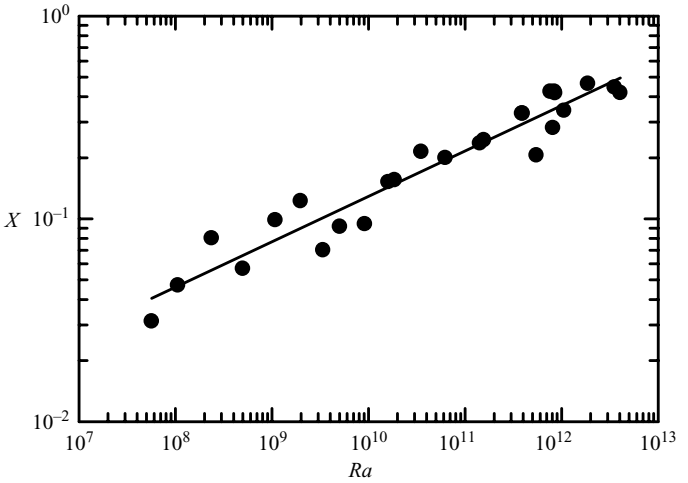

FIGURE 5. Log-log plot of *Ra*-dependence of the spatial-averaged X measured inside the bottom plate. The solid line represents a power law fit with a slope of 0.22.

Libchaber 1996). Table 1 lists the values of S_T and $S_{T'}$ for the data shown in figure 2. It is seen that these quantities have opposite signs at the two plates but their product is of the same sign at both plates. Moreover, their magnitude is approximately the same for both plates. It has been shown previously that the so-called ramp–cliff (i.e. slow rise followed by sharp fall) structures that exist in the time series of passive scalars would give rise to S_T and $S_{T'}$ of opposite signs (Sreenivasan & Antonia 1977), while active scalars, such as the temperature field in thermal turbulence, that exhibit cliff–ramp structures (believed to correspond to thermal plumes) would produce S_T and $S_{T'}$ of the same sign (Belmonte & Libchaber 1996). From table 1 we see that S_T and $S_{T'}$ indeed have the same sign in both top and bottom plates, indicating the presence of cliff–ramp structures. Note that because we measure temperature deficit due to plume emissions the signs of S_T and $S_{T'}$ inside the plates are opposite to those in the fluid (Belmonte & Libchaber 1996). Table 1 also shows that the value of $S_T S_{T'}$ is larger for large *Ra*. Because the level of plume emission should increase with increasing *Ra*, we may therefore use the quantity $X \equiv S_T S_{T'}$ as a measure of the strength of plume emissions from the plates. Figure 5 plots X as a function of *Ra*, obtained from temperature signals measured inside the bottom plate where data for all aspect ratios are available which gives a wide range in *Ra*. In the figure the spatial

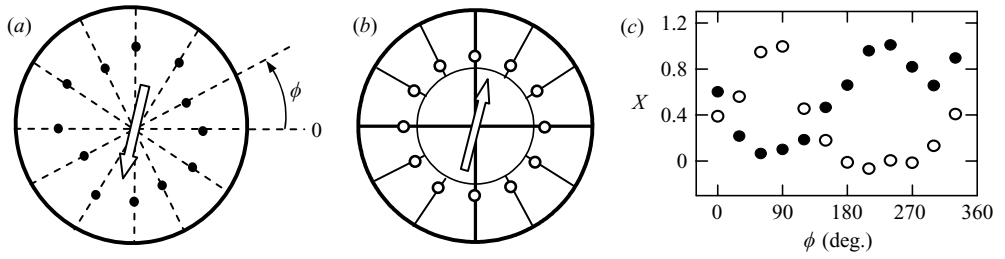

FIGURE 6. Plume emission patterns obtained by multi-probes embedded in the conducting plates. Open arrows indicate the direction of the LSC below the top plate (*a*) and above the bottom plate (*b*). The positions of the embedded thermistors are shown as dots and circles for the top and bottom plates respectively, with their azimuth ϕ indicated. (*c*) Angular variation of X for top (dots) and bottom plate (circles) ($Ra = 3.9 \times 10^{11}$, $\Gamma = 1$).

average of X from 12 thermistors is used (see figure 6). It is therefore reasonably representative of the overall strength of plume emissions from the plate. It appears that at this level of accuracy X shows no apparent dependence on the aspect ratio Γ and it increases monotonically with Ra. The log-log plot reveals that within the level of data scatter X has an approximate power-law dependence on Ra over about 5 decades of the parameter range. A fit shown as the solid line gives an exponent 0.22. We are not aware of any theoretical prediction of the intensity of plume emissions. Here we offer a somewhat speculative explanation. We note that the strength of plume emission should increase with the Nusselt number. If we take X to be proportional to Nu then the exponent 0.22 is rather close to the value of 1/5 predicted by Grossmann & Lohse (2000) as the exponent for region I_u in the (Ra, Pr) phase plane.

We now examine the spatial distribution of plume emissions. Twelve thermistors were selected from each plate to study the plume-emission pattern. These are arranged with an equal angular spacing of 30° on each plate, as shown in figures 6(*a*) and 6(*b*) for the top and bottom plates respectively. The thermistors in the top plate are located between 25 and 30 cm from the plate centre, and those of the bottom plate are on a circle of 30 cm radius. Figure 6(*c*) shows the the angular variation of X for both top and bottom plates, where ϕ is the azimuth of the thermistors as indicated in figure 6(*a*). One can see clearly that X in both plates has an approximately sinusoidal distribution and that the distributions in the two plates have a phase difference of $\sim 180°$. It has been found recently that the circulation plane of the LSC in an $\Gamma = 1$ convection cell has a preferred azimuthal orientation (Sun, Xia & Tong 2005*b*; Brown, Nikolaenko & Ahlers 2005; Xi *et al.* 2006). In the present work we determined this orientation by placing thermistors near the sidewall (at mid-height) of the cell. Because the LSC is a band with a width spanning half of the cell diameter (Lui & Xia 1998) and because of the technique used, its direction is determined only approximately (to within a range of $\pm 20°$) and this is indicated by the thick arrows in figures 6(*a*) and 6(*b*) respectively for flows near the top and bottom plates (top views). From figure 6(*a*) it is seen that the largely horizontal LSC just below the top plate would make a downward turn at $\phi \approx 240°$; this is also the angle where X is maximum as shown in figure 6(*c*) which is where more downward cold plumes are emitted compared to positions of smaller X. Similarly, at the bottom plate it is seen from figure 6(*b*) that the LSC makes an upward turn around $\phi \approx 60°$–$90°$, coinciding with the region where X is maximum inside the bottom plate. This shows that as a result of its interaction with the LSC plume emission is no longer uniform across the plates; rather it exhibits

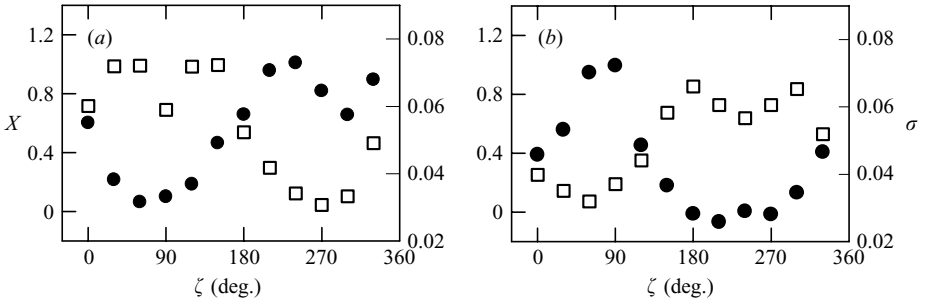

FIGURE 7. Angular dependence of X and σ for top (a) and bottom (b) plates ($Ra = 3.9 \times 10^{11}$). Circles, X; squares, σ.

a spatial pattern that reflects the orientation of the LSC above (below) the plates. One can also see from figure 6(c) that the value of X is roughly the same for both plates, which indicates top–bottom symmetry. It should be mentioned that the same pattern in X is also observed for the 12 thermistors located on the outer circle shown in figure 1(b), i.e. close to the perimeter of the bottom plate. For the inner circles, no detailed pattern is observed because there are only 4 thermistors.

From figure 6(c) we can see that where X is maximum in a plate it is minimum in the opposite plate, and that the region of minimum X is also where plumes from the other plate arrive. This shows that plume emissions are suppressed in regions of a plate that are being impinged by plumes from the opposite plate. This suppression occurs because the arrival of cold (hot) plumes cools down (warms up) the bottom (top) plates, thus reducing the instability that presumably triggers plume emissions. However, the regions of suppressed plume emissions are not 'quiet' regions in terms of temperature fluctuations. This is illustrated in figure 7, where we plot the angular dependence of both X and the RMS temperature σ for the top and the bottom plates. It is seen that X and σ appear to be out of phase by 180°, i.e. at places where X is maximum σ is minimum. Also, the maximum value of σ is about twice as large as the minimum σ. This result is surprising at first but may be understood as follows. From figure 6 we see that the region of minimum X is where plumes from the opposite plate arrive and this is the region where plume mixing takes place: it is the mixing of hot and cold plumes that produces large temperature fluctuations. In regions of maximum X plume emission is enhanced and only one type of plume exists, so temperature fluctuations are relatively small and σ is only about half that where plume mixing dominates. As already mentioned, Cioni *et al.* (1997) were able to determine the azimuthal orientation of the LSC in mercury convection based on the short-time averaged temperature of the embedded probes. In our case, however, we find that the mean temperatures of embedded thermistors do not exhibit an obvious spatial pattern, which has to be revealed by higher-order statistical quantities of the temperature. We believe the difference is most likely caused by the very different fluid properties (or Pr) in the two experiments. Because of its large heat capacity and thermal conductivity, the emission of a mercury thermal plume will produce a much larger temperature change in the plate than in the case of water. Indeed, in the mercury experiment time-averaged temperature among the embedded thermistors varied by between 4 % and 5% of the global mean within one plate, while in our case it is only about 1%. In absolute terms, the maximum variation is ~ 1.3°C ($Ra = 3.5 \times 10^8$) in mercury and ~ 0.5°C ($Ra = 3.9 \times 10^{11}$) in water.

4. Conclusion

Using embedded temperature probes in the top and bottom plates of a 1 m diameter convection cell, we are able to detect emissions of plumes and of plume clusters. We find that the product $S_T S_{T'}$ of the temperature skewness S_T and the skewness of the temperature time derivative $S_{T'}$ may be used as a measure of the intensity of plume emissions. It is found that the quantity X $(= S_T S_{T'})$ appears to have a power-law dependence on Ra, i.e. $X \sim Ra^{0.22}$. With the aid of multiple embedded probes, we find that X in the plates exhibits a pattern that corresponds well to the orientation of the larger-scale circulation in the convecting flow. By comparing the spatial distribution of X and that of the RMS temperature σ, we further find that the maximum temperature fluctuations take place in regions dominated by plume mixing instead of regions of plume emission. It is also found that temperature fluctuations inside the plates and at the cell centre have approximately the same scaling dependence on the Rayleigh number Ra. These findings suggest that temperature fluctuations inside the conducting plates have the same statistical and scaling properties as those in the cell interior and that the spatial distribution of plume emissions is highly inhomogeneous and corresponds to that of the LSC in the cell. These results also suggest that the statistical and scaling properties of the temperature field in the convecting fluid and the orientation of the LSC can be measured non-intrusively by probes imbedded inside the plates, which may be useful in certain situations such as convection in high-pressure gas and in liquid metals. Previous studies of the velocity and temperature fields in the convecting fluid have suggested that plume emissions from the top and bottom plates are synchronized via the bulk fluid (Qiu & Tong 2001; Sun *et al.* 2005*b*). By measuring temperatures inside the plates, the present study provides direct evidence that plume emissions become synchronized both spatially and temporally with convective flow in the cell interior. Finally we point out that because of the high thermal conductivity of the copper plates relative to water, the temperature distribution in the plates is rather uniform and that higher-order statistical moments of temperature have to be used to reveal the flow pattern and the spatial distribution of plume emissions. In this respect the method presented in this paper may be used as a non-invasive diagnostic tool in situations where it is either not possible or undesirable to place probes inside the system.

We gratefully acknowledge support of this work by the Research Grants Council of Hong Kong SAR under Grant No. CUHK 403003 and 403705. KQX wishes to acknowledge the support of a Croucher Senior Research Fellowship by the Croucher Foundation of Hong Kong.

REFERENCES

Belmonte, A. & Libchaber, A. 1996 Thermal signature of plumes in turbulent convection: The skewness of the derivative. *Phys. Rev.* E **53**, 4893–4898.

Bershadskii, A., Niemela, J. J., Praskovsky, A. & Sreenivasan, K. R. 2004 Clusterization and intermittency of temperature fluctuations in turbulent convection. *Phys. Rev. E* **69**, 056314.

Brown, E., Nikolaenko, A. & Ahlers, G. 2005*a* Reorientation of the large-scale circulation in turbulent Rayleigh-Bénard convection. *Phys. Rev. Lett.* **95**, 084503.

Brown, E., Nikolaenko, A., Funfschilling, D. & Ahlers, G. 2005*b* Heat transport in turbulent Rayleigh-Bénard convection: Effect of finite top- and bottom-plate conductivity. *Phys. Fluids* **17**, 075108.

Castaing, B., Gnuaratne, G., Heslot, F, Kadanoff, L., Libchaber, A., Thomae, S., Wu, X. Z., Zaleski, S. & Zanetti, G. 1989 Scaling of hard thermal turbulence in Rayleigh-Bénard turbulent convection. *J. Fluid Mech.* **204**, 1–30.

Chaumat, S., Castaing, B. & Chillà, F. 2002 Rayleigh-Bénard cells: Influence of the plate properties. *Advances in Turbulence IX: Proc. 9th European Turbulence Conference* (ed. I. P. Castro, P. E. Hancock & T. G. Thomas). CIMNE, Barcelona.

Ching, E. S. C., Guo, H., Shang, X.-D., Tong, P. & Xia, K.-Q. 2004 Extraction of plumes in turbulent thermal convection. *Phys. Rev. Lett.* **93**, 124501.

Cioni, S., Ciliberto, S. & Sommeria, J. 1997 Strongly turbulent Rayleigh-Bénard convection in mercury: comparison with results at moderate Prandtl number. *J. Fluid Mech.* **335**, 111–140.

Funfschilling, D. & Ahlers, G. 2004 Plume motion and large-scale circulation in a cylindrical Rayleigh-Bénard cell. *Phys. Rev. Lett.* **92**, 194502.

Grossmann, S. & Lohse, D. 2000 Scaling in thermal convection: A unifying theory. *J. Fluid Mech.* **407**, 27–56.

Hunt, J. C. R., Vrieling, A. J., Nieuwstadt, F. T. M. & Fernando, H. J. S. 2003 The influence of the thermal diffusivity of the lower boundary on eddy motion in convection. *J. Fluid Mech.* **491**, 183–205.

Krishnamurti, R. & Howard, L. N. 1981 Large-scale flow generation in turbulent convection. *Proc. Natl Acad.* **78** (4), 1981–1985.

Lui, S.-L. & Xia, K.-Q. 1998 Spatial structure of the thermal boundary layer in turbulent convection. *Phys. Rev.* E **57**, 5494–5503.

Parodi, A., Hardenberg, J., Passoni, G., Provenzale, A. & Spiegel, E. A. 2004 Clustering of Plumes in Turbulent Convection. *Phys. Rev. Lett.* **92**, 194503.

Qiu, X.-L. & Tong, P. 2001 Onset of coherent oscillations in turbulent Rayleigh-Bénard convection. *Phys. Rev. Lett.* **87**, 094501.

Sreenivasan, K. R. & Antonia, R.A. 1977 Skewness of temperature derivatives in turbulent shear flows. *Phys. Fluids* **20**, 1986–1988.

Sun, C., Ren, L.-Y., Song, H. & Xia, K.-Q. 2005*a* Heat transport by turbulent Rayleigh-Bénard convection in 1 m diameter cylindrical cells of widely varying aspect ratio. *J. Fluid Mech.* **542**, 165–174.

Sun, C., Xia, K.-Q. & Tong, P. 2005*b* Three-dimensional flow structures and dynamics of turbulent thermal convection in a cylindrical cell. *Phys. Rev.* E **72**, 026302.

Verzicco, R. 2004 Effects of nonperfect thermal sourses in turbulent thermal convection. *Phys. Fluids* **16**, 1965–1979.

Xi, H.-D., Lam, S. & Xia, K.-Q. 2004 From laminar plumes to organized flows: the onset of large-scale circulation in turbulent thermal convection. *J. Fluid Mech.* **503**, 47–56.

Xi, H.-D., Zhou, Q. & Xia, K.-Q. 2006 Azimuthal motion of the mean wind in turbulent thermal convection. *Phys. Rev.* E **73**, 056312.

Xia, K.-Q. & Lui, S.-L. 1997 Turbulent thermal convection with an obstructed sidewall. *Phys. Rev. Lett.* **79**, 5006–5009.

Zhou, S.-Q. & Xia, K.-Q. 2002 Plume statistics in thermal turbulence: mixing of an active scalar. *Phys. Rev. Lett.* **89**, 184502.